Phase Separation Modulates the Formation and Stabilities of DNA Guanine Quadruplex

Zi Gao, Jun Yuan, Xiaomei He, Handing Wang, and Yinsheng Wang*

Cite This: JACS Au 2023, 3, 1650−1657

Read Online

ACCESS | 📊 Metrics & More | 📖 Article Recommendations | 🆂🅸 Supporting Information

ABSTRACT: In the presence of monovalent alkali metal ions, G-rich DNA sequences containing four runs of contiguous guanines can fold into G-quadruplex (G4) structures. Recent studies showed that these structures are located in critical regions of the human genome and assume important functions in many essential DNA metabolic processes, including replication, transcription, and repair. However, not all potential G4-forming sequences are actually folded into G4 structures in cells, where G4 structures are known to be dynamic and modulated by G4-binding proteins as well as helicases. It remains unclear whether there are other factors influencing the formation and stability of G4 structures in cells. Herein, we showed that DNA G4s can undergo phase separation *in vitro*. In addition, immunofluorescence microscopy and ChIP-seq experiments with the use of BG4, a G4 structure-specific antibody, revealed that disruption of phase separation could result in global destabilization of G4 structures in cells. Together, our work revealed phase separation as a new determinant in modulating the formation and stability of G4 structures in human cells.

KEYWORDS: guanine quadruplex, phase separation, transcription regulation, transcription factor, ChIP-seq
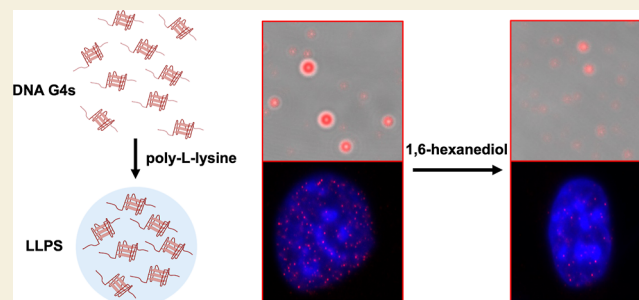
INTRODUCTION

Guanine quadruplexes (G4s) are non-canonical DNA structures composed of two or more layers of G-tetrads, each of which contains four guanines stabilized by Hoogsteen base pairing and a monovalent metal ion, *e.g.*, K^+ and Na^+. The formation of G4 structures in human cells was first reported in 1987,[1] and many subsequent studies were conducted to assess G4 formation *in vitro* and in cells. In particular, it was revealed bioinformatically and experimentally that DNA G4 is ubiquitously present in the human genome.[2−4] These studies also unveiled the enrichment of G4 structures at replication origins, oncogene promoters, and telomeres, suggesting the important functions of G4 structures in regulating DNA replication, transcription, telomere maintenance, and other biological processes.[5]

G4 structures are highly dynamic in cells,[6,7] and effective regulations of G4s are crucial for maintaining genomic and epigenetic stability, as manifested by the functions of known G4-binding proteins in chromatin remodeling (*e.g.*, ATRX and REV1),[8,9] long-range DNA interactions (*e.g.*, YY1 and CTCF),[10,11] and genetic diseases (*e.g.*, WRN and BLM).[12,13] Moreover, G4 structures are known to be dynamic during cell cycle progression, where higher levels of G4 structures were observed in S-phase cells.[14] Therefore, it is important to understand how G4 structures are regulated in cells.

Liquid−liquid phase separation (LLPS) promotes the formation of membraneless compartments in cells, such as nucleolus, nuclear speckles, Cajal bodies, processing bodies (P bodies), stress granules, *etc*.[15] LLPS has been shown to participate in a wide range of cellular processes, including transcription, translation, DNA damage repair, cell signaling, and spatial genome organization.[15−17] Although many studies are focused on LLPS of proteins or protein compartments, it was recently revealed that, in the absence of proteins, DNA can also undergo phase separation. For instance, Shakya and King[18] found that certain sequences of DNA, *e.g.*, poly(GC), can form phase-separated condensates. In addition, recent studies on G4-binding proteins unveiled important functions of G4s in many different biological processes.[19−21] Interestingly, many of these proteins, including FUS,[22] hnRNPA1,[23] hnRNPA2,[24] and YY1,[25] can undergo phase separation. Furthermore, G4 structures can promote the condensation of G4-binding proteins, including histone H1 and SERBP1.[26,27]

In light of these previous studies, we hypothesized that phase separation may modulate the stabilities of G4 structures in cells. In this study, we observed LLPS of DNA G4s *in vitro* and demonstrated that phase-separated G4 DNA droplets can

be disintegrated by 1,6-hexanediol (1,6-HD), an agent known to disrupt LLPS.[28,29] We also found that disruption of phase separation diminished the enrichment of G4 structures in chromatin of cultured human cells.

■ METHODS

Cell Culture

U2OS human osteosarcoma cells were cultured in Dulbecco's modified Eagle's medium (DMEM, Thermo Fisher) supplemented with 10% fetal bovine serum (FBS, Thermo Fisher) and 1% penicillin−streptomycin solution (PS, GE Healthcare) at 37 °C with 5% CO_2.

Oligodeoxyribonucleotides and G4 Formation

Unlabeled and 5′-TAMRA-labeled oligodeoxyribonucleotides (ODNs) were purchased from Integrated DNA Technologies (IDT), and their sequences are listed in Supporting Information, Table S1. These ODNs were annealed in a buffer containing 10 mM Tris−HCl (pH 7.5), 10 mM KCl, and 0.1 mM EDTA by heating to 95 °C for 5 min, followed by cooling down to room temperature slowly over 6 h.

Circular Dichroism Spectroscopy

The circular dichroism (CD) spectra for the ODNs (10 μM) in a binding buffer containing 10 mM HEPES (pH 7.4) and 0.1 mM EDTA with or without 0.1 mg/mL poly-L-lysine (P2636, Sigma) were recorded at room temperature on a Jasco-815 spectrometer (Easton, MD) at a scan rate of 1 nm/s. The CD spectra were averaged from the signal of two repetitive scans collected in the wavelength range of 220−320 nm. The final spectra were obtained by the subtraction of the signal acquired for the buffer solution and signal smoothing and plotted using GraphPad Prism.

Phase Separation Assay

Pre-annealed 5′-TAMRA-labeled DNA and unlabeled DNA were mixed at a molar ratio of 1:50 in the above-mentioned buffer. For imaging of DNA in the presence of NaCl, NaCl was added to the buffer until its desired concentration was reached. The samples were incubated with or without 0.1 mg/ml poly-L-lysine at 25 °C for 30 min. The samples were subsequently dropped onto a glass microscope slide and covered with a 12 mm coverslip (CG15NH1, Thorlabs) immediately before imaging. Fluorescence and differential interference contrast (DIC) imaging was conducted on an LSM 880 upright confocal microscope (Carl Zeiss) with a 60× objective. The images were analyzed by ZEN software.

Turbidity Measurements

Unlabeled *cMYC* DNA (20 μM) was prepared under the same conditions as in phase separation assay. After incubation, the absorbance at 400 nm was measured using a Nanodrop One spectrophotometer (Thermo Scientific). Triplicate measurements were performed. The average of the three readouts for each replicate was recorded.

1,6-Hexanediol Treatment

In all *in vitro* assays, including phase separation and turbidity measurements, stock solutions of 20, 40, and 60% of 1,6-hexanediol (240117, Sigma) in a binding buffer were prepared before treatment. After the addition of an equal volume of 1,6-HD-containing buffer, the sample solution was mixed thoroughly by pipetting and incubated at 25 °C for another 30 min before measurement.

G4 Immunofluorescence

U2OS cells were treated with 6% 1,6-hexanediol (240117, Sigma) prepared in DMEM for 1 min; JQ1 (HY-13030, MedChemExpress) was added to U2OS cells until its final concentration reached 1.0 μM, and the cells were incubated for 12 h before immunofluorescence microscopy imaging. The immunofluorescence microscopy experiments were performed following previously published procedures.[14] Briefly, cells on the coverslip were fixed in methanol/acetic acid (3:1, v/v) for 10 min, permeabilized with 0.1% triton-X100/PBS for 15

min, and treated with 50 μg/mL RNase A (EN0531, Thermo Fisher). After blocking with 2% BSA at room temperature for 1 h, immunofluorescence microscopy experiments were conducted using standard methods with BG4 (MABE917, Sigma-Aldrich), anti-FLAG (14793S, Cell Signaling Technology), and anti-rabbit Alexa 594-conjugated (A11037, Invitrogen) antibodies. Nuclei were stained with DAPI (D9542, Sigma). Finally, the coverslips were mounted with ProLong Diamond Antifade Mountant (Invitrogen). Images were recorded using an LSM880 confocal laser scanning microscope (Carl Zeiss) with a 100× objective and analyzed with ZEN. The foci number per nucleus were counted using Find maxima in ImageJ. The graphs were plotted using GraphPad Prism8.

G4-ChIP Sequencing and qPCR

G4-ChIP sequencing was performed using the custom-purified BG4 antibody and conducted as previously described with minor modifications.[30] DNA was fragmented following the protocol described previously.[31] Briefly, chromatin samples were diluted in a blocking buffer containing 25 mM HEPES (pH 7.5), 10.5 mM NaCl, 110 mM KCl, 1 mM $MgCl_2$, and 1% BSA and treated with RNase A. The chromatin sample was subsequently incubated with 500 ng of the BG4 antibody with rotation at 1400 rpm for 1.5 h at 16 °C. To the mixture were then added 5 μL of pre-blocked Anti-Flag M2 magnetic beads (Sigma, M8823), and the suspension was incubated under the same conditions for 1 h. After washing with ice-cold wash buffer (10 mM Tris, pH 7.4, 100 mM KCl, 0.1% Tween 20) 7 times, the captured DNA was eluted with TE buffer containing Proteinase K while rotating at 1400 rpm. (6 h, 65 °C). The eluted DNA was then purified by DNA Clean and Concentrator-5 (Zymo).

The DNA-sequencing library was prepared using NEBNext Ultra DNA Library Prep Kit for Illumina (NEB) following the manufacturer's instructions. The quantity and quality of the purified DNA libraries were assessed by a Qubit and an Agilent 2100 Bioanalyzer. The samples were multiplexed for next-generation sequencing on an MGISEQ-2000 platform (BGI).

For quantitative PCR, immunoprecipitated samples and the input control were used to quantify the enrichment of G4 structures. qPCR was carried out using Luna Universal qPCR Master Mix (NEB) on a CFX96 touch real-time PCR detection system (Bio-Rad). The primers are listed in Supporting Information, Table S1.

Cell Counting Kit-8 Assay. The cell cytotoxicity after 1,6-HD and JQ1 treatment was analyzed by using cell counting kit-8 (CK04, Dojindo) following the manufacturer's protocols. Cells were seeded at a density of 5×10^3/well in 100 μL of medium into 96-well microplates. Cells were incubated overnight before treatment. After treatment, 10 μL of the cell counting kit-8 (CCK-8) reagent was added to each well and then incubated for 3 h. The absorbance was then measured at 450 nm using a BioTek Synergy H1 microplate reader. All experiments were performed in triplicate.

Bioinformatics Analysis

FastQC (version 0.11.9) was employed for the quality assessment of ChIP-seq data, and the reads were subsequently mapped to the human hg38 reference genome using Bowtie2 (Version 2.5.0).[32] The two replicates were merged using SAMtools for analysis.[33] The unaligned and repeated reads were filtered out, and the remaining reads were subjected to peak calling using MACS2 (v2.2.7.1)[34] with a false discovery rate of 0.05. Bigwig files were generated by using the bamCompare tool.[35] The results were visualized using Integrative Genomics Viewer (IGV).[36]

ChIP-seq data sets of transcription factors (TFs) were retrieved from the ChIP-atlas portal (https://chip-atlas.org/) using "hg38", experiment type "ChIP: TFs and others", cell type class "bone", threshold for significance "50", and cell type "U2OS". Experiments with treatment or genetic manipulation were removed from analysis. BG4 peaks that can be detected in both control and 1,6-hexanediol-treated cells were separated into "augmented G4" and "diminished G4" based on the enrichment score. The overlapping percentage of G4 with TF binding sites was calculated using bedtools.[37] Fold change was defined as the ratio between TF binding sites' overlapping percentage with "augmented G4" and "diminished G4" in 1,6-
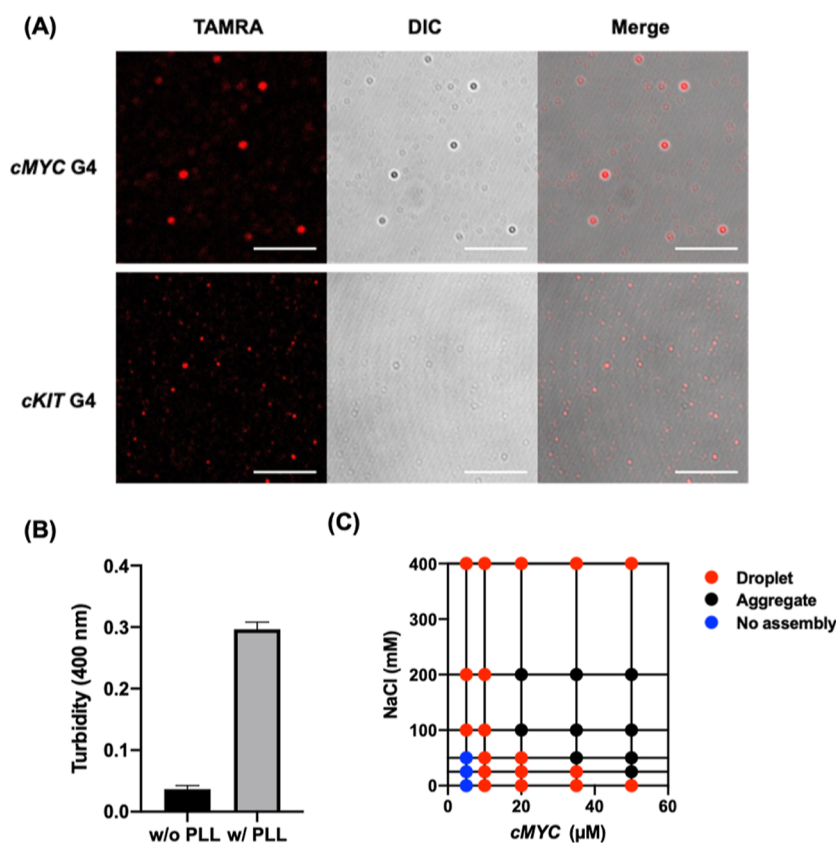
Figure 1. G4 DNA undergoes phase separation *in vitro*. (A) Images of 10 μM mixture of 5′-TAMRA-labeled and unlabeled (1:50) G4 oligodeoxynucleotides acquired from fluorescence microscopy and differential interference contrast (DIC) microscopy (scale bar = 10 μm). (B) Turbidity of 10 μM G4 DNA derived from the *cMYC* promoter in the presence or absence of 2 μM PLL. (C) Matrix diagram showing the phase separation of different concentrations of c*MYC* G4 DNA in the presence of various concentrations of NaCl. Droplets are round shaped, whereas aggregates are of irregular shape (Figure S2).

hexanediol- *vs* mock-treated cells. Profiles and heatmaps were generated by using the computeMatrix tool.[35] The ChIP-seq data reported in this paper are available at the NCBI GEO repository under accession number GSE225772.

■ RESULTS AND DISCUSSION

To investigate whether G4s undergo phase separation and assemble into droplets in the absence of proteins, we tested two different G4-forming sequences derived from the promoter regions of c*MYC* and c*KIT* proto-oncogenes. In this vein, the *cKIT* promoter harbors three G4-forming sequences,[38] and the first sequence, KIT1, was used in the present study. Oligodeoxynucleotides were pre-annealed in a buffer containing 10 mM KCl and confirmed by circular dichroism spectroscopy (Figure S1) to ensure the formation of G4 structures before the LLPS assays. As depicted in Figure 1A, both G4 sequences can undergo phase separation and assemble into droplets in the presence of poly-L-lysine (PLL), a cationic polymer used for studying phase separation,[39] where droplets start to form at 10 μM G4 DNA. We also examined G4 droplet formation by using a previously reported turbidity assay.[26,40] Upon incubation with PLL, the turbidity of the DNA sample increased significantly, as manifested by the formation of droplets in PLL-containing DNA solution (Figure 1B).

We next assessed the influence of salt concentration on phase separation of G4 DNA. Our results showed that, after annealing G4 DNA in a K$^+$-containing buffer, the droplets started to form at DNA concentrations as low as 10 μM (Figure 1C). At a low concentration (5 μM), G4 DNA does not assemble into droplets until NaCl concentration is at least 100 mM (Figure S2). We also observed that, at higher DNA concentrations (20−50 μM), G4 DNA assembles into droplets at both low and high NaCl concentrations but forms aggregates at intermediate NaCl concentrations (Figures 1C and S2). We reason that the addition of salt increases the ionic strength of the solution and attenuated the electrostatic repulsions between negatively charged G4 DNA, thereby resulting in droplet formation at low DNA concentration and aggregation at high DNA concentration.[41] Further increases in salt concentration augmented the solubility of DNA in the PLL−DNA mixture;[42] as a result, we observed precipitate dissolution and droplet reformation at high salt concentrations. Together, we showed that G4 DNA can undergo phase separation at a concentration as low as 10 μM. In this respect, it is worth noting that the intracellular concentration of Na$^+$ is about 10−15 mM, residing in the low concentration range of NaCl used in this study.[43] In addition, the average local concentration of DNA in metaphase chromosomes is approximately 0.17 g/mL,[44] which is much higher than the 10 μM G4 DNA probe used in the current study ($\sim$7*10^{-5} g/mL). Thus, DNA in chromatin experiences an environment with much more molecular crowding, which favors LLPS,[45] than the *in vitro* conditions employed in the current study.

1,6-HD has been frequently employed to disrupt phase separation through inhibition of hydrophobic interactions.[28,29]
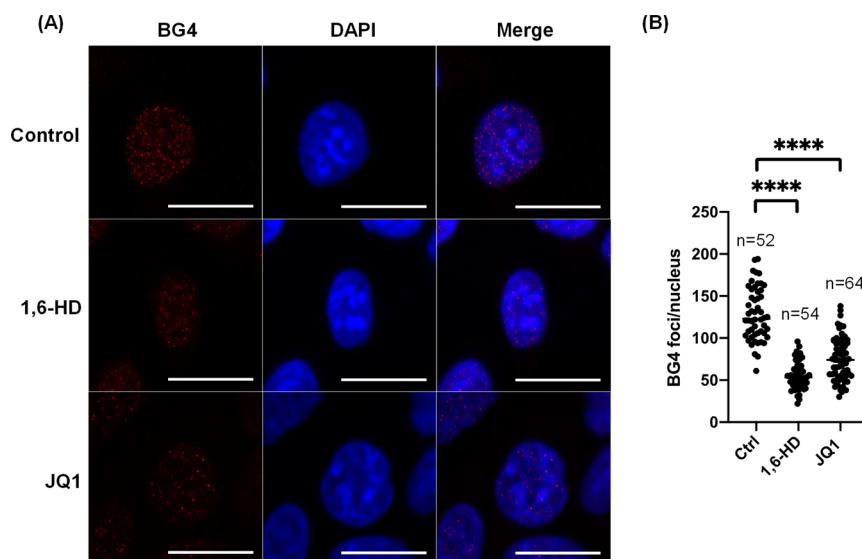
Figure 2. Disruption of phase separation led to diminished G4 structure foci in cells. (A) Immunofluorescence microscopy images showing the presence of G4 structure foci in the control, as well as in 1,6-HD- and JQ1-treated U2OS cells. Nuclei were stained with DAPI; and G4 structures were monitored using the BG4 antibody (scale bar = 20 μm). (B) Quantification of G4 structure foci after 1,6-HD and JQ1 treatment. The p values were calculated by using two-tailed, unpaired Student's t-test: ****, $p < 0.0001$.
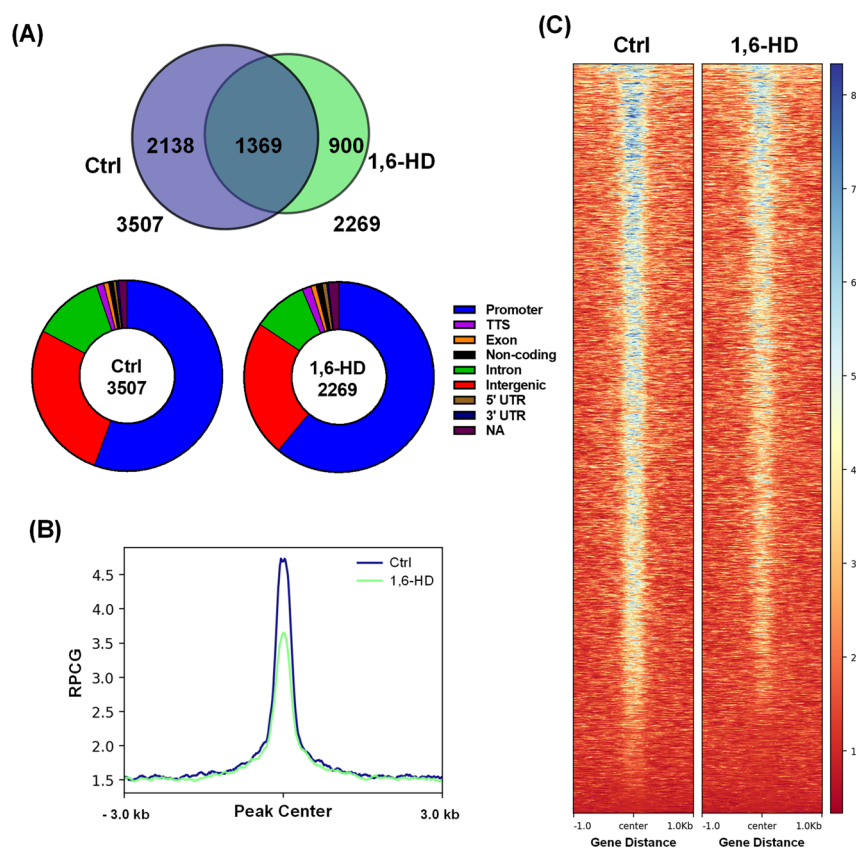
Figure 3. BG4 ChIP-seq results of U2OS cells with and without 1,6-HD treatment. (A) Venn diagram depicting the numbers of significant BG4 ChIP-seq peaks in U2OS cells with (1,6-HD) or without (Ctrl) 1,6-HD treatment, and pie charts showing gene annotation of these peaks. (B) Genome-wide profiles of BG4 ChIP-seq peaks for control and 1,6-HD-treated cells showing diminished peak intensity after 1,6-HD treatment. (C) Heatmap of peak distribution and intensity in control and 1,6-HD-treated cells.

We found that the addition of 1,6-HD led to disintegration of G4 DNA droplets (Figure S3A), where we observed a marked attenuation in droplet size when the solution contained 20% 1,6-HD. We also assessed droplet disruption by using a turbidity assay. As displayed in Figure S3B, treatment with increasing concentrations of 1,6-HD led to decreased turbidity of the DNA solution, underscoring the disintegration and/or dissolution of G4 DNA droplets. As 1,6-HD exhibits a more pronounced impact on turbidity at a low NaCl concentration than a high concentration, phase separation of G4 DNA at a
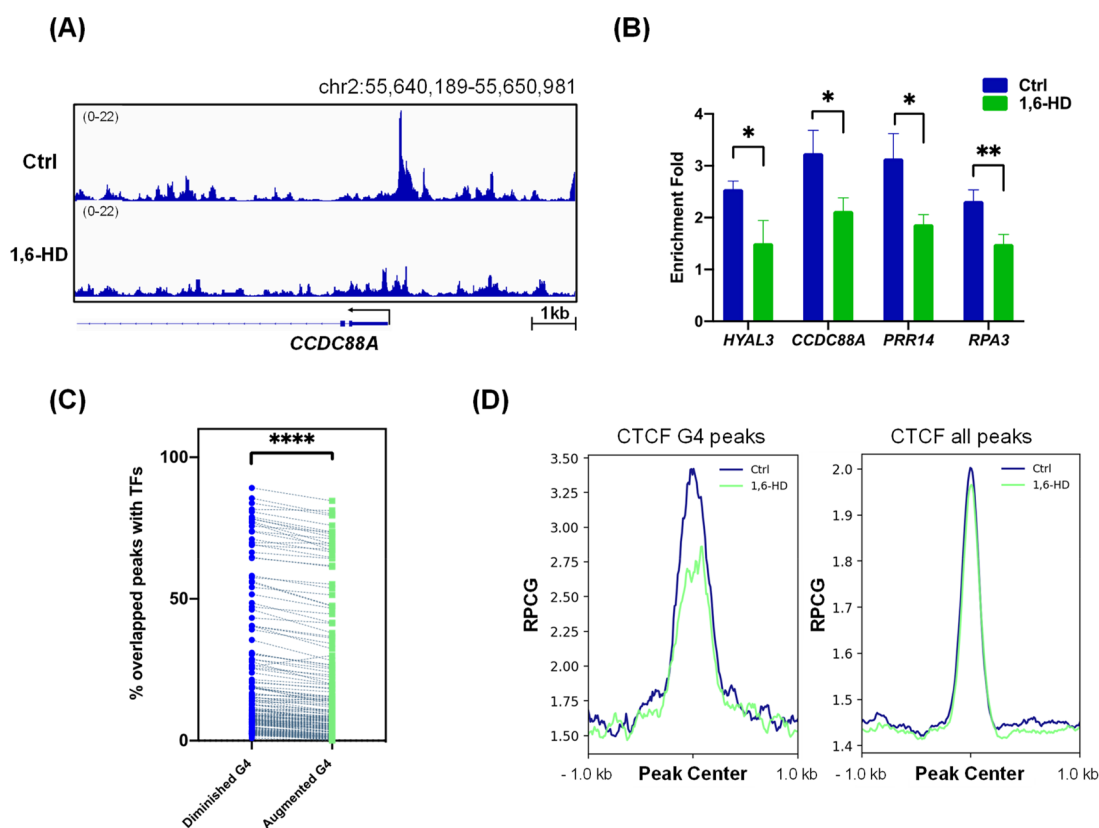
Figure 4. 1,6-HD treatment led to diminished G4 structures in cells. (A) ChIP-seq tracks showing the transcription start site (TSS) of the *CCDC88A* gene in control and 1,6-HD-treated U2OS cells. (B) ChIP-qPCR results showing diminished enrichment of G4 structures in the promoter regions of *HYAL3*, *CCDC88A*, *PRR14*, and *RPA3* genes in U2OS cells upon 1,6-HD treatment. The enrichment was assessed using primers derived from the genomic regions around the TSS where the BG4 ChIP-seq peaks are located. *ESR1*, which has no G4 peak in the promoter region, served as a negative control to calculate the changes in enrichment fold. The data represent mean ± S.D. of results from three independent experiments. The p values were calculated by using two-tailed, unpaired Student's t-test: *, $p < 0.05$; **, $0.001 \leq p < 0.01$. (C) Comparison of overlapping percentages of TF occupancy at G4 sites in control and 1,6-HD-treated cells. Dash lines connect the same TFs in both groups. The p values were calculated by using two-tailed, paired Student's t-test: ****, $p < 0.0001$. (D) Profiles of fold enrichment of G4 signals in control and 1,6-HD-treated cells at CTCF-binding sites with G4 structures and all CTCF binding sites, respectively.

low NaCl concentration depends more on hydrophobic interaction. This result demonstrated that, aside from electrostatic interaction, hydrophobic interaction also contributes to LLPS of G4 DNA. Together, these results revealed that 1,6-HD treatment promotes the disintegration of G4 droplets *in vitro*.

We next investigated how phase separation influences the stability of G4 structures in cells. To this end, we treated U2OS cells with 6% 1,6-HD for 1 min and assessed G4 formation in cells by using immunofluorescence microscopy with the use of the BG4 antibody.[14] In line with the *in vitro* observations, we detected pronounced diminutions in G4 structure foci in cells upon 1,6-HD treatment (Figure 2). In this context, 1,6-HD is known to be capable of disrupting protein−protein interactions;[46] hence, the diminished G4 levels in cells may also arise partly from attenuated protein−protein interactions involving G4-binding proteins. It is of note that 1,6-HD exposure did not appreciably influence the survival of U2OS cells (Figure S4A).

Several studies demonstrated the formation of G4s in promoters of transcriptionally active genes.[47−49] In addition, transcription co-activators form liquid-like condensates, which recruit other proteins to enhancer regions to activate transcription.[50,51] Therefore, we hypothesized that the assembly of these phase-separated condensates associated with promoter regions may lead to stabilization of G4 structures. To test this hypothesis, we assessed how G4 formation in cells is perturbed upon treatment with JQ1, which disrupts the binding of BRD4 to H3K27ac-marked enhancer chromatin and dissolves the phase-separated condensates composed of mediators and RNA polymerase II at super-enhancers.[51] Immunofluorescence microscopy analysis with the use of the BG4 antibody again revealed a significant diminution in BG4 foci in U2OS cells after JQ1 treatment (Figure 2). In this regard, we observed that a 12 h treatment with 1.0 μM JQ-1 did not alter the survival of U2OS cells (Figure S4B). This result substantiated our conclusion that G4 structures in cells are stabilized in phase-separated condensates, although attenuated enhancer activity, arising from JQ-1 treatment, may also contribute in part to diminished G4 structures.

To further examine the roles of phase separation in stabilizing G4 structures in cells, we performed BG4-ChIP-seq experiment for U2OS cells that were untreated or treated with 1.5% 1,6-HD for 2 min.[30,31] Our results from two biological replicates revealed a substantially diminished number of BG4 ChIP-seq peaks, namely, from 3507 peaks in control cells to 2269 peaks in 1,6-HD-treated cells. The majority of the peaks (58.9 and 61% in control and 1,6-HD-treated cells, respectively) are located in promoter regions

(Figure 3A), which is in agreement with the previously reported results.[48] We also observed that the peak intensities were substantially attenuated upon 1,6-HD treatment (Figure 3B,C). It is worth noting that, among the 1369 overlapped peaks detected from control and 1,6-HD-treated cells, more than 65% of the peaks are located in promoter regions.

We further validated the BG4 ChIP-seq data by using ChIP-qPCR. We chose several genes, including *HYAL3*, *CCDC88A*, *PRA3*, and *PRR14*, whose promoter regions exhibit high G4-forming potential and display diminished BG4 ChIP-seq peak intensities following 1,6-HD treatment (Figures 4A,B, S5). Consistent with the ChIP-seq results, we detected attenuated enrichment of G4 structures in the promoter regions of all four genes upon 1,6-HD treatment. Hence, we conclude that phase separation contributes to the stabilization of G4 structures in cells.

Because G4 structures were found to be binding hubs for TFs in chromatin,[48] we next examined whether those loci with G4 structures being sensitive to 1,6-HD treatment are enriched with TF binding sites. To this end, we first divided those G4 loci commonly detected in control and 1,6-HD-treated cells into two groups based on IP enrichment scores, *i.e.*, those G4 loci exhibiting decreased and increased BG4 ChIP signals after 1,6-HD treatment (*i.e.*, labeled in Figure 4C as "diminished G4" and "augmented G4", respectively). We subsequently calculated the overlapping percentage of BG4 peaks in each group with ChIP-seq results of TFs using publicly available data from ChIP-Atlas. Our results showed that those loci with a diminished BG4 signal upon 1,6-HD treatment are more likely to co-localize with TF binding sites than those with an elevated BG4 signal after 1,6-HD treatment (Figure 4C). Along this line, it remains unclear how 1,6-HD treatment leads to elevated BG4 signals in some genomic regions, although we speculate that this may arise from augmented accessibilities of G4 structures in chromatin of these genomic regions. A comparison of BG4 ChIP-seq peaks detected in control and 1,6-HD-treated cells with respect to individual ChIP-seq data of TFs, including CTCF, MYC, and ZBTB48, showed minimal or no effects of their overall genome-wide occupancy upon 1,6-HD treatment (Figures 4D and S6). We, however, observed pronounced diminutions in enrichment of these TFs at those binding sites enriched with G4 structures. These data suggest that G4-mediated LLPS is involved in regulating the chromatin occupancy of TFs.

CONCLUSIONS

In summary, we demonstrated that G4 DNA can undergo phase separation, and disruption of phase separation leads to genome-wide destabilization of G4s. Previous studies showed that DNA G4 structures promote phase separation through binding to phase-separated proteins.[52] Here, we revealed another mechanism in modulating dynamic formation of DNA G4 structures, which may bear important implications in transcriptional regulation. In this vein, G4 structures are enriched in gene promoters,[5] and RNA polymerase II can partition into two distinct types of phase-separated condensates, where the form with the C-terminal domain being hypophosphorylated is accompanied with transcription initiation, but the hyperphosphorylated form is associated with the splicing complex.[53] While more efforts are needed to understand further how phase separation of G4 DNA regulates biological processes, our studies suggest that G4 structures are hubs of not only the transcription machinery[48] but perhaps also other molecular complexes involved in chromatin remodeling and long-range DNA interactions.[7,10,25]

ASSOCIATED CONTENT

Ⓢ Supporting Information

The Supporting Information is available free of charge at https://pubs.acs.org/doi/10.1021/jacsau.3c00106.

Sequences and primers, CD spectra, droplet formation, DNA G4 droplets disrupted by 1,6-HD treatment, CCK-8 cytotoxicity assay results, IGV plots, and profiles of G4 signals (PDF)

AUTHOR INFORMATION

Corresponding Author

Yinsheng Wang — *Department of Chemistry, University of California Riverside, Riverside, California 92521-0403, United States; Environmental Toxicology Graduate Program, University of California Riverside, Riverside, California 92521-0403, United States;* ⓞ orcid.org/0000-0001-5565-283X; Email: Yinsheng.Wang@ucr.edu

Authors

Zi Gao — *Department of Chemistry, University of California Riverside, Riverside, California 92521-0403, United States*

Jun Yuan — *Environmental Toxicology Graduate Program, University of California Riverside, Riverside, California 92521-0403, United States*

Xiaomei He — *Department of Chemistry, University of California Riverside, Riverside, California 92521-0403, United States*

Handing Wang — *Department of Chemistry, University of California Riverside, Riverside, California 92521-0403, United States*

Complete contact information is available at:
https://pubs.acs.org/10.1021/jacsau.3c00106

Notes

The authors declare no competing financial interest.

ACKNOWLEDGMENTS

REFERENCES

(1) Henderson, E.; Hardin, C. C.; Walk, S. K.; Tinoco, I., Jr.; Blackburn, E. H. Telomeric DNA oligonucleotides form novel intramolecular structures containing guanine-guanine base pairs. *Cell* **1987**, *51*, 899−908.

(2) Huppert, J. L.; Balasubramanian, S. Prevalence of quadruplexes in the human genome. *Nucleic Acids Res.* **2005**, *33*, 2908−2916.

(3) Todd, A. K.; Johnston, M.; Neidle, S. Highly prevalent putative quadruplex sequence motifs in human DNA. *Nucleic Acids Res.* **2005**, *33*, 2901−2907.

(4) Zheng, K. W.; Zhang, J. Y.; He, Y. D.; Gong, J. Y.; Wen, C. J.; Chen, J. N.; Hao, Y. H.; Zhao, Y.; Tan, Z. Detection of genomic G-quadruplexes in living cells using a small artificial protein. *Nucleic Acids Res.* **2020**, *48*, 11706−11720.

(5) Bedrat, A.; Lacroix, L.; Mergny, J. L. Re-evaluation of G-quadruplex propensity with G4Hunter. *Nucleic Acids Res.* **2016**, *44*, 1746−1759.

(6) Di Antonio, M.; Ponjavic, A.; Radzevicius, A.; Ranasinghe, R. T.; Catalano, M.; Zhang, X.; Shen, J.; Needham, L. M.; Lee, S. F.; Klenerman, D.; Balasubramanian, S. Single-molecule visualization of

DNA G-quadruplex formation in live cells. *Nat. Chem.* **2020**, *12*, 832−837.

(7) Hansel-Hertsch, R.; Beraldi, D.; Lensing, S. V.; Marsico, G.; Zyner, K.; Parry, A.; Di Antonio, M.; Pike, J.; Kimura, H.; Narita, M.; Tannahill, D.; Balasubramanian, S. G-quadruplex structures mark human regulatory chromatin. *Nat. Genet.* **2016**, *48*, 1267−1272.

(8) Teng, Y. C.; Sundaresan, A.; O'Hara, R.; Gant, V. U.; Li, M.; Martire, S.; Warshaw, J. N.; Basu, A.; Banaszynski, L. A. ATRX promotes heterochromatin formation to protect cells from G-quadruplex DNA-mediated stress. *Nat. Commun.* **2021**, *12*, 3887.

(9) Eddy, S.; Ketkar, A.; Zafar, M. K.; Maddukuri, L.; Choi, J. Y.; Eoff, R. L. Human Rev1 polymerase disrupts G-quadruplex DNA. *Nucleic Acids Res.* **2014**, *42*, 3272−3285.

(10) Li, L.; Williams, P.; Ren, W.; Wang, M. Y.; Gao, Z.; Miao, W.; Huang, M.; Song, J.; Wang, Y. YY1 interacts with guanine quadruplexes to regulate DNA looping and gene expression. *Nat. Chem. Biol.* **2021**, *17*, 161−168.

(11) Tikhonova, P.; Pavlova, I.; Isaakova, E.; Tsvetkov, V.; Bogomazova, A.; Vedekhina, T.; Luzhin, A. V.; Sultanov, R.; Severov, V.; Klimina, K.; Kantidze, O. L.; Pozmogova, G.; Lagarkova, M.; Varizhuk, A. DNA G-Quadruplexes Contribute to CTCF Recruitment. *Int. J. Mol. Sci.* **2021**, *22*, 7090.

(12) Wu, W. Q.; Hou, X. M.; Li, M.; Dou, S. X.; Xi, X. G. BLM unfolds G-quadruplexes in different structural environments through different mechanisms. *Nucleic Acids Res.* **2015**, *43*, 4614−4626.

(13) Kamath-Loeb, A. S.; Loeb, L. A.; Johansson, E.; Burgers, P. M.; Fry, M. Interactions between the Werner Syndrome Helicase and DNA Polymerase δ Specifically Facilitate Copying of Tetraplex and Hairpin Structures of the d(CGG) Trinucleotide Repeat Sequence. *J. Biol. Chem.* **2001**, *276*, 16439−16446.

(14) Biffi, G.; Tannahill, D.; McCafferty, J.; Balasubramanian, S. Quantitative visualization of DNA G-quadruplex structures in human cells. *Nat. Chem.* **2013**, *5*, 182−186.

(15) Hirose, T.; Ninomiya, K.; Nakagawa, S.; Yamazaki, T. A guide to membraneless organelles and their various roles in gene regulation. *Nat. Rev. Mol. Cell Biol.* **2022**, *24*, 288−304.

(16) Boeynaems, S.; Alberti, S.; Fawzi, N. L.; Mittag, T.; Polymenidou, M.; Rousseau, F.; Schymkowitz, J.; Shorter, J.; Wolozin, B.; Van Den Bosch, L.; Tompa, P.; Fuxreiter, M. Protein phase separation: A new phase in cell biology. *Trends Cell Biol.* **2018**, *28*, 420−435.

(17) Ong, J. Y.; Torres, J. Z. Phase separation in cell division. *Mol. Cell* **2020**, *80*, 9−20.

(18) Shakya, A.; King, J. T. DNA local-flexibility-dependent assembly of phase-separated liquid droplets. *Biophys. J.* **2018**, *115*, 1840−1847.

(19) Gao, Z.; Williams, P.; Li, L.; Wang, Y. A quantitative proteomic approach for the identification of DNA guanine quadruplex-binding proteins. *J. Proteome Res.* **2021**, *20*, 4919−4924.

(20) Huang, Z. L.; Dai, J.; Luo, W. H.; Wang, X. G.; Tan, J. H.; Chen, S. B.; Huang, Z. S. Identification of G-quadruplex-binding protein from the exploration of RGG motif/G-quadruplex interactions. *J. Am. Chem. Soc.* **2018**, *140*, 17945−17955.

(21) Zhang, X.; Spiegel, J.; Martinez Cuesta, S.; Adhikari, S.; Balasubramanian, S. Chemical profiling of DNA G-quadruplex-interacting proteins in live cells. *Nat. Chem.* **2021**, *13*, 626−633.

(22) Yagi, R.; Miyazaki, T.; Oyoshi, T. G-quadruplex binding ability of TLS/FUS depends on the beta-spiral structure of the RGG domain. *Nucleic Acids Res.* **2018**, *46*, 5894−5901.

(23) Ghosh, M.; Singh, M. RGG-box in hnRNPA1 specifically recognizes the telomere G-quadruplex DNA and enhances the G-quadruplex unfolding ability of UP1 domain. *Nucleic Acids Res.* **2018**, *46*, 10246−10261.

(24) Wang, F.; Tang, M. L.; Zeng, Z. X.; Wu, R. Y.; Xue, Y.; Hao, Y. H.; Pang, D. W.; Zhao, Y.; Tan, Z. Telomere- and telomerase-interacting protein that unfolds telomere G-quadruplex and promotes telomere extension in mammalian cells. *Proc. Natl. Acad. Sci. U. S. A.* **2012**, *109*, 20413−20418.

(25) Wang, W.; Qiao, S.; Li, G.; Cheng, J.; Yang, C.; Zhong, C.; Stovall, D. B.; Shi, J.; Teng, C.; Li, D.; Sui, G. A histidine cluster determines YY1-compartmentalized coactivators and chromatin elements in phase-separated enhancer clusters. *Nucleic Acids Res.* **2022**, *50*, 4917−4937.

(26) Mimura, M.; Tomita, S.; Shinkai, Y.; Hosokai, T.; Kumeta, H.; Saio, T.; Shiraki, K.; Kurita, R. Quadruplex folding promotes the condensation of linker histones and DNAs via liquid-liquid phase separation. *J. Am. Chem. Soc.* **2021**, *143*, 9849−9857.

(27) Liu, X.; Xiong, Y.; Zhang, C.; Lai, R.; Liu, H.; Peng, R.; Fu, T.; Liu, Q.; Fang, X.; Mann, S.; Tan, W. G-quadruplex-induced liquid-liquid phase separation in biomimetic protocells. *J. Am. Chem. Soc.* **2021**, *143*, 11036−11043.

(28) Liu, X.; Jiang, S.; Ma, L.; Qu, J.; Zhao, L.; Zhu, X.; Ding, J. Time-dependent effect of 1,6-hexanediol on biomolecular condensates and 3D chromatin organization. *Genome Biol.* **2021**, *22*, 230.

(29) Strom, A. R.; Emelyanov, A. V.; Mir, M.; Fyodorov, D. V.; Darzacq, X.; Karpen, G. H. Phase separation drives heterochromatin domain formation. *Nature* **2017**, *547*, 241−245.

(30) Hansel-Hertsch, R.; Spiegel, J.; Marsico, G.; Tannahill, D.; Balasubramanian, S. Genome-wide mapping of endogenous G-quadruplex DNA structures by chromatin immunoprecipitation and high-throughput sequencing. *Nat. Protoc.* **2018**, *13*, 551−564.

(31) Tang, F.; Wang, Y.; Gao, Z.; Guo, S.; Wang, Y. Polymerase *η* Recruits DHX9 Helicase to Promote Replication across Guanine Quadruplex Structures. *J. Am. Chem. Soc.* **2022**, *144*, 14016−14020.

(32) Langmead, B.; Salzberg, S. L. Fast gapped-read alignment with Bowtie 2. *Nat. Methods* **2012**, *9*, 357−359.

(33) Danecek, P.; Bonfield, J. K.; Liddle, J.; Marshall, J.; Ohan, V.; Pollard, M. O.; Whitwham, A.; Keane, T.; McCarthy, S. A.; Davies, R. M.; Li, H. Twelve years of SAMtools and BCFtools. *Gigascience* **2021**, *10*, giab008.

(34) Zhang, Y.; Liu, T.; Meyer, C. A.; Eeckhoute, J.; Johnson, D. S.; Bernstein, B. E.; Nusbaum, C.; Myers, R. M.; Brown, M.; Li, W.; Liu, X. S. Model-based analysis of ChIP-seq (MACS). *Genome Biol.* **2008**, *9*, R137.

(35) Ramírez, F.; Ryan, D. P.; Grüning, B.; Bhardwaj, V.; Kilpert, F.; Richter, A. S.; Heyne, S.; Dündar, F.; Manke, T. deepTools2: a next generation web server for deep-sequencing data analysis. *Nucleic Acids Res.* **2016**, *44*, W160−W165.

(36) Robinson, J. T.; Thorvaldsdottir, H.; Winckler, W.; Guttman, M.; Lander, E. S.; Getz, G.; Mesirov, J. P. Integrative genomics viewer. *Nat. Biotechnol.* **2011**, *29*, 24−26.

(37) Quinlan, A. R.; Hall, I. M. BEDTools: a flexible suite of utilities for comparing genomic features. *Bioinformatics* **2010**, *26*, 841−842.

(38) Ducani, C.; Bernardinelli, G.; Hogberg, B.; Keppler, B. K.; Terenzi, A. Interplay of Three G-Quadruplex Units in the KIT Promoter. *J. Am. Chem. Soc.* **2019**, *141*, 10205−10213.

(39) Vieregg, J. R.; Lueckheide, M.; Marciel, A. B.; Leon, L.; Bologna, A. J.; Rivera, J. R.; Tirrell, M. V. Oligonucleotide-Peptide Complexes: Phase Control by Hybridization. *J. Am. Chem. Soc.* **2018**, *140*, 1632−1638.

(40) Alberti, S.; Gladfelter, A.; Mittag, T. Considerations and Challenges in Studying Liquid-Liquid Phase Separation and Biomolecular Condensates. *Cell* **2019**, *176*, 419−434.

(41) Flock, S.; Labarbe, R.; Houssier, C. Dielectric constant and ionic strength effects on DNA precipitation. *Biophys. J.* **1996**, *70*, 1456−1465.

(42) Leng, M.; Felsenfeld, G. The preferential interactions of polylysine and polyarginine with specific base sequences in DNA. *Proc. Natl. Acad. Sci. U.S.A.* **1966**, *56*, 1325−1332.

(43) Fleysher, L.; Oesingmann, N.; Brown, R.; Sodickson, D. K.; Wiggins, G. C.; Inglese, M. Noninvasive quantification of intracellular sodium in human brain using ultrahigh-field MRI. *NMR Biomed.* **2013**, *26*, 9−19.

(44) Daban, J. R. Physical constraints in the condensation of eukaryotic chromosomes. Local concentration of DNA versus linear packing ratio in higher order chromatin structures. *Biochemistry* **2000**, *39*, 3861−3866.

(45) Andre, A. A. M.; Spruijt, E. Liquid-liquid phase separation in crowded environments. *Int. J. Mol. Sci.* **2020**, *21*, 5908.

(46) Lin, Y.; Mori, E.; Kato, M.; Xiang, S.; Wu, L.; Kwon, I.; McKnight, S. L. Toxic PR Poly-Dipeptides Encoded by the C9orf72 Repeat Expansion Target LC Domain Polymers. *Cell* **2016**, *167*, 789−802 e12.

(47) Lago, S.; Nadai, M.; Cernilogar, F. M.; Kazerani, M.; Dominiguez Moreno, H.; Schotta, G.; Richter, S. N. Promoter G-quadruplexes and transcription factors cooperate to shape the cell type-specific transcriptome. *Nat. Commun.* **2021**, *12*, 3885.

(48) Spiegel, J.; Cuesta, S. M.; Adhikari, S.; Hansel-Hertsch, R.; Tannahill, D.; Balasubramanian, S. G-quadruplexes are transcription factor binding hubs in human chromatin. *Genome Biol.* **2021**, *22*, 117.

(49) Li, C.; Wang, H.; Yin, Z.; Fang, P.; Xiao, R.; Xiang, Y.; Wang, W.; Li, Q.; Huang, B.; Huang, J.; Liang, K. Ligand-induced native G-quadruplex stabilization impairs transcription initiation. *Genome Res.* **2021**, *31*, 1546−1560.

(50) Sabari, B. R.; Dall'Agnese, A.; Boija, A.; Klein, I. A.; Coffey, E. L.; Shrinivas, K.; Abraham, B. J.; Hannett, N. M.; Zamudio, A. V.; Manteiga, J. C.; Li, C. H.; Guo, Y. E.; Day, D. S.; Schuijers, J.; Vasile, E.; Malik, S.; Hnisz, D.; Lee, T. I.; Cisse, I. I.; Roeder, R. G.; Sharp, P. A.; Chakraborty, A. K.; Young, R. A. Coactivator condensation at super-enhancers links phase separation and gene control. *Science* **2018**, *361*, No. eaar3958.

(51) Cho, W. K.; Spille, J. H.; Hecht, M.; Lee, C.; Li, C.; Grube, V.; Cisse, I. I. Mediator and RNA polymerase II clusters associate in transcription-dependent condensates. *Science* **2018**, *361*, 412−415.

(52) Jack, A.; Kim, Y.; Strom, A. R.; Lee, D. S. W.; Williams, B.; Schaub, J. M.; Kellogg, E. H.; Finkelstein, I. J.; Ferro, L. S.; Yildiz, A.; Brangwynne, C. P. Compartmentalization of telomeres through DNA-scaffolded phase separation. *Dev. Cell* **2022**, *57*, 277−290 e9.

(53) Guo, Y. E.; Manteiga, J. C.; Henninger, J. E.; Sabari, B. R.; Dall'Agnese, A.; Hannett, N. M.; Spille, J. H.; Afeyan, L. K.; Zamudio, A. V.; Shrinivas, K.; Abraham, B. J.; Boija, A.; Decker, T. M.; Rimel, J. K.; Fant, C. B.; Lee, T. I.; Cisse, I. I.; Sharp, P. A.; Taatjes, D. J.; Young, R. A. Pol II phosphorylation regulates a switch between transcriptional and splicing condensates. *Nature* **2019**, *572*, 543−548.